# Enhanced anisotropic magnetoresistance in the odd-parity multipole-ordered conductor Ba$_{1-x}$K$_x$Mn$_2$As$_2$

Takuya Aoyama [1], Masahiro Kudo,[1] Kaoru Igarashi,[1] Kazutoshi Emi,[1] Shojiro Kimura,[2] Yoshinori Imai [1], and Kenya Ohgushi[1]

^{1}*Department of Physics, Graduate School of Science, Tohoku University, 6-3 Aramaki-Aoba, Aoba-ku, Sendai, Miyagi 980-8578, Japan*
^{2}*Institute for Materials Research, Tohoku University, Sendai, Miyagi 980-8577, Japan*

We examined the magnetoresistance with applied magnetic field in the *ab* plane for Ba$_{1-x}$K$_x$Mn$_2$As$_2$ with $x = $ 0–0.30, which exhibits a unique antiferromagnetic order with the simultaneous breaking of spatial-inversion and time-reversal symmetries. By investigating the temperature and magnetic-field strength/direction dependence of the magnetoresistance in detail, we found there are three main contributions to the magnetoresistance. One is due to an external field effect inducing cyclotron motion of electron and Zeeman splitting. This is most prominent at $x = 0$ and 0.15. The second one is a spin fluctuation related negative magnetoresistance. This becomes large at a ferromagnetic transition temperature of 100 K at $x = 0.25$. The third one is the spin-orbit coupling related effects, which leads to an in-plane anisotropy of magnetoresistance. We also argue that anisotropic magnetoresistance can be understood in terms of the magnetoelectric effect arising from the odd-parity magnetic-multipole ordering.

I. INTRODUCTION

Recently, anomalous magnetotransport phenomena have been observed in metals with the odd-parity magnetic-multipole order. The examples include the second-order nonlinear conductivity in CuMnAs [1], the current-induced magnetization in UNi$_4$B [2], and the current-induced piezoelectric response in EuMnBi$_2$ [3]. These phenomena are induced by an asymmetric distortion of the Fermi surface, which are introduced by the odd-parity magnetic-multipole order through the spin-orbit coupling [4]. The development of new target materials as well as the exploration of novel magnetotransport phenomena will give a new route to study functionalities in metals with the odd-parity magnetic-multipole orders.

BaMn$_2$As$_2$ with ThCr$_2$Si$_2$ structure (space group $I4/mmm$ and lattice constant $a = 4.17$ Å, $c = 13.5$ Å) shows a G-type antiferromagnetic magnetism below Néel temperature ($T_{\rm N}$) of 625 K [5]. An important feature of BaMn$_2$As$_2$ is the simultaneous breaking of the spatial-inversion and time-reversal symmetry due to its antiferromagnetic order [5–8]. The crystal and magnetic structures of BaMn$_2$As$_2$ are shown in Fig. 1(a). An inversion operation transforms the blue MnAs$_4$ tetrahedron (tetrahedron A) into the red MnAs$_4$ tetrahedron (tetrahedron B), which have a different coordination environment. In the paramagnetic phase, the A and B tetrahedra are linked together by the spatial-inversion operation with the Ba site as the inversion center; as a result, the global spatial-inversion symmetry is preserved. In the antiferromagnetic phase, however, A and B tetrahedra have reversed spin directions along the c axis at their centers. Since the spin direction is invariant under the spatial-inversion operation, the antiferromagnetic phase no longer holds the global

spatial-inversion symmetry. In addition, the time-reversal symmetry is also broken in the antiferromagnetic phase, resulting in a simultaneous breaking of the spatial inversion and time-reversal symmetries in the antiferromagnetic phase of BaMn$_2$As$_2$. The magnetic point group in the magnetically ordered phase is $4'/m'mm'$, where $'$ is the time-reversal operation. In the magnetic point group, a magnetic quadrupole and a magnetic hexadecapole with the odd-parity nature are considered to be ordered in a ferroic manner [9]. This is actually demonstrated by the observation and analysis of the second harmonic generation of lights [10].

Upon hole doping into BaMn$_2$As$_2$ via K substitution for Ba, the insulating state is immediately collapsed, and the metallic conductivity is observed at whole temperatures for $x > 0.016$ in Ba$_{1-x}$K$_x$Mn$_2$As$_2$ [11,12]. The G-type antiferromagnetism is, however, rather robust against the hole doping, and the $T_{\rm N}$ is as high as 500 K at $x = 0.40$ [13]. Intriguingly, for $x = 0.40$, a ferromagnetic moment of ~ 0.4 $\mu_{\rm B}$/Mn appears along the *ab* plane with $T_{\rm C} \sim 100$ K [14–16] [Fig. 1(b)]. The microscopic mechanism of this ferromagnetism is controversial at present; the x-ray magnetic circular dichroism and the nuclear magnetic resonance experiments indicate that itinerant holes of As-$4p$ orbitals contribute to the ferromagnetism [15,16], while first-principle calculations based on the density functional theory indicate that Mn spins show the canted ferromagnetism due to the double exchange interaction between the mobile holes and the localized spins [17]. When the ferromagnetic order is superimposed on the odd-parity magnetic-multipole order, unique magnetotransport phenomena are expected to emerge owing to a strong internal magnetic field generated by the spontaneous magnetization.
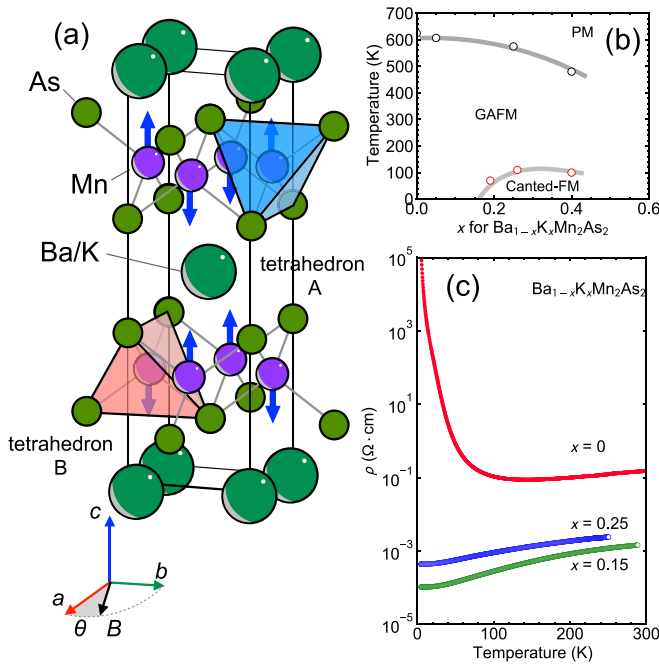
224422-1

FIG. 1. (a) Crystal and magnetic structures of $Ba_{1-x}K_xMn_2As_2$. The definition of the crystal axes and the magnetic field rotation plane in the anisotropic magnetoresistance measurements are shown. (b) The magnetic phase diagram of $Ba_{1-x}K_xMn_2As_2$ illustrated with reference to Refs. [11,13,15]. The PM, GAFM, FM indicate paramagnetic, G-type antiferromagnetic, and ferromagnetic states, respectively. (c) The temperature dependence of ρ at zero magnetic field of $Ba_{1-x}K_xMn_2As_2$.

In this study we investigated magnetotransport under the rotating magnetic field in the *ab* plane for $Ba_{1-x}K_xMn_2As_2$ with $x = 0$–0.30. We found that the magnetoresistance shows a rich variety as a function of composition, temperature, and magnetic-field directions. In particular, we observed the large anisotropic magnetoresistance in an antiferromagnetic insulating phase of $x = 0$ and the ferromagnetic metallic phase of $x = 0.25$. We interpret these phenomena in terms of three contributions: (1) the positive magnetoresistance induced by an external magnetic field, (2) the negative magnetoresistance induced by the suppressed spin fluctuations, and (3) the positive magnetoresistance induced by a spin-orbit coupling. We also discuss the anisotropic magnetoresistance in terms of a linear magnetoelectric effect arising from the odd-parity magnetic-multipole order.

II. EXPERIMENT

Single crystals of $Ba_{1-x}K_xMn_2As_2$ were grown using the MnAs self-flux method. The elements of Ba (Sigma-Aldrich, purity 4N), K (Sigma-Aldrich, purity 3.5N), Mn (Rare-metallic chemistry, purity 3N or 5N), and As (Kojundo Chemical Laboratory, purity 3N or 5N) were used as the starting materials. The raw materials with the molar ratio of Ba : K : Mn : As $= 1 - x : x : 4 : 4$ were mixed under an argon atmosphere in a glove box, and were placed in an alumina crucible. The crucible was sealed in a stainless-steel tube under the argon atmosphere. The materials were sintered at 1000 °C

for 4 h, and were cooled down to 840 °C for 25–90 h. We obtained the platelike single crystals with $0.8 \times 0.5 \times 0.02 \text{ mm}^3$ as a typical dimension. The chemical formula of the resulting crystals was evaluated by using SEM-EDX (JSM-6500F, JEOL Ltd.) and a typical standard deviation of composition x within one crystal is ±0.03. In the following, x represents not the nominal but the estimated value. The electrical resistivity (ρ) was measured by the four-terminal method with an electric current (J) applied along the 100 direction in a ^{4}He cryostat. The limited sample thickness along the c axis prohibits us from measuring resistivity in the $J \parallel 001$ configuration. To collect an angle dependence of magnetoresistance, the single crystal was rotated in the superconducting magnet generating a magnetic field (B) of 17.5 T. A commercial magnetometer (MPMS, Quantum Design) was used to measure the magnetization.

III. RESULTS

A. Electrical resistivity and magnetization

The temperature dependence of the ρ for $x = 0$, 0.15, and 0.25 are shown in Fig. 1(c). $BaMn_2As_2$ ($x = 0$) exhibits metallic electrical conduction near room temperature due to the hole carriers with high mobility caused by the strong hybridization of Mn $3d_{xy}$ and As $4p_z$ orbitals. A metal-insulator crossover is observed around 100 K, and the ground state is the antiferromagnetic insulator. This crossover is most likely due to the change in conduction characteristics from a coherent to a hopping conduction, as the mobility is suppressed on cooling [18,19]. In fact, in the intermediate temperature range (30–100 K), the temperature dependence of the ρ can be well fitted using the small polaron hopping model of $\rho = \rho_0 T^{3/2} \exp(\Delta/k_B T)$ with $\Delta = 27$ meV, where k_B is Boltzmann's constant and Δ is the hopping gap [Fig. 2(c)]. Upon further cooling, a kink in the temperature derivative of the electrical resistivity is observed at $T^\star \sim 20$ K [Fig. 2(b)]. Below $T^\star$, the temperature dependence of the electrical resistivity can be well fitted by the three-dimensional variable range hopping model of $\rho = \rho_0 \exp(T_0/T)^{1/4}$ with $T_0 = 1.1 \times 10^6$ K [Fig. 2(c)]. This observation indicates that electrons move by a quantum tunneling rather than a thermal hopping below $T^\star$, because the hopping level of electrons became deeper with cooling [11,20,21]. The $T^\star$ anomaly is also captured as the enhancement of NMR relaxation rate $1/T_1$ [22]. Such changes in the conduction mechanism have a significant impact on the magnetotransport as described below.

Whereas $BaMn_2As_2$ has an insulating ground state, a metallic conductivity is observed over the whole temperature range for $x = 0.15$ and 0.25, indicating the hole doping suppresses the formation of the localized state [Figs. 1(c) and 3(a)]. With increasing x, the absolute value of ρ increases and the residual-resistivity ratio (RRR) tends to be small. This observation indicates that the coherence of itinerant electrons is reduced at heavily doped regions for certain reasons such as the randomness caused by K substitution and/or the degradation of samples by humidity.

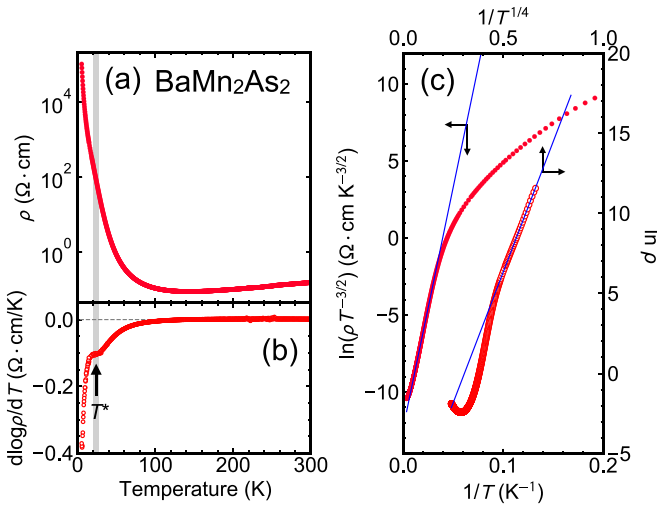Figure 3(c) represents the temperature dependence of the magnetization in the *ab* plane for $x = 0.13$ and 0.25. We

FIG. 2. (a) The temperature dependence of the resistivity (ρ) at zero magnetic field of $BaMn_2As_2$. (b) Temperature dependence of $d\log\rho/dT$ of $BaMn_2As_2$. The $T^\star$ indicates a temperature with a small anomaly in ρ. The detail of $T^\star$ anomaly is described in the main text. (c) The fitting of $\ln(\rho T^{-3/2})$ against $1/T$ and $\ln\rho$ against $1/T^{1/4}$, corresponding to the small polaron and the variable-range hopping model, respectively.
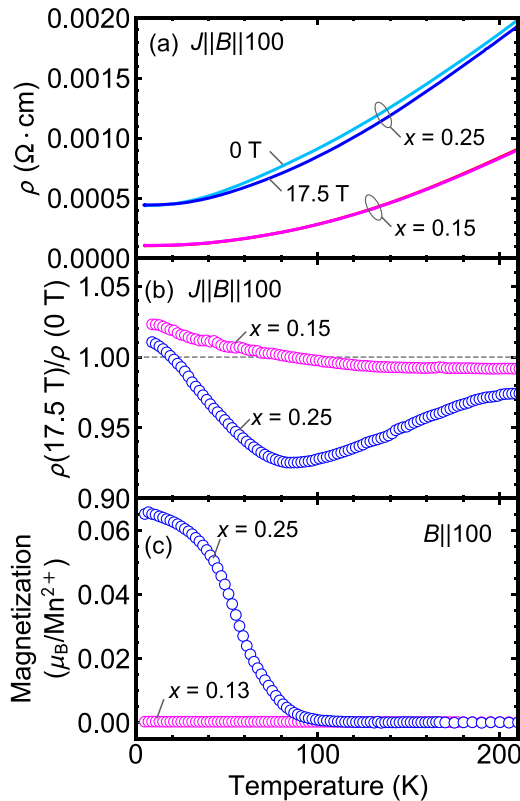

FIG. 3. (a) Temperature dependence of the resistivity (ρ) at $B = 0$ T (magenta for $x = 0.15$ and cyan for $x = 0.25$) and $B = 17.5$ T (red for $x = 0.15$ and blue for $x = 0.25$) for $Ba_{1-x}K_xMn_2As_2$. Note that ρ at $B = 0$ and 17.5 T are almost identical in $x = 0.15$. (b) Temperature dependence of $\rho(17.5\,\text{T})/\rho(0\,\text{T})$ with the configuration of $J||B||100$. (c) Temperature dependence of the in-plane magnetization at $B = 0.01$ T.

observed no sizable magnetization for $x = 0.13$, as in the case of $BaMn_2As_2$. In contrast, a sharp increase in magnetization below 100 K is observed at $x = 0.25$, indicating a ferromagnetic transition. The spontaneous magnetization is as large as $0.06 \mu_B/Mn$ at 5 K. This ferromagnetic transition temperature as well as the magnetization value are consistent with the previous studies [11,15].

B. Temperature dependence of magnetoresistance

In order to evaluate the effect of the magnetic field on the charge transport, we measured ρ under the magnetic field with the longitudinal configuration [Fig. 3(a)], where the current and the magnetic field of $B = 17.5$ T are applied along the 100 direction. The data presented here are collected in the warming run, and the data for $x = 0$ could not be taken owing to its insulating nature. The data at 0 T and those at 17.5 T are almost overlapping with each other for $x = 0.15$ and 0.25, indicating the moderate impact of the magnetic field on the charge dynamics. However, if one plots the magnetoresistance ratio $\rho(17.5\,\text{T})/\rho(0\,\text{T})$ as in Fig. 3(b), one can see the sizable magnetoresistance. For $x = 0.15$, the negative magnetoresistance of less than 1% at room temperature changes its sign at 100 K on cooling, and the positive magnetoresistance reaches its maximum values of about 3% at 4.2 K. For $x = 0.25$, a negative magnetoresistance at room temperature is about 3%, which is larger than that in $x = 0.15$. This negative magnetoresistance increases with cooling, and its magnitude reaches up to 8% at 100 K. Further cooling suppressed the negative MR, and a positive magnetoresistance of about 1% is observed at the lowest temperature.

C. Magnetic field dependence of magnetoresistance

Figures 4(a)–4(c) represent the isothermal magnetoresistance in the wide magnetic field range up to 17.5 T; the data are taken in a longitudinal configuration with the current and magnetic field along the 100 direction. In $x = 0$, the largest magnetoresistance was observed among three compositions measured in this study; note that the vertical axis scale in Fig. 4(a) is different from those for the other two compositions shown in Figs. 4(b) and 4(c). The negative magnetoresistance, which is proportional to the square of the magnetic field, is observed at 150 K, and its amplitude develops with cooling down to 40 K. However, the magnetoresistance exhibits a complicated behavior below $T^\star \sim 20$ K. There appears a positive component, which is dominant particularly in the low magnetic field, while the negative component is still dominant in the high magnetic field. Both the negative and positive magnetoresistance grow with further cooling. At 5 K, the negative and positive magnetoresistance becomes comparable at 9 T, resulting in a peak structure with the maximum value of 25%. In $x = 0.15$ [Fig. 4(b)], the monotonic field dependence proportional to the square of the magnetic field is observed in the whole temperature range measured. The magnetoresistance changes its sign from a negative to a positive one on cooling across 120 K. The maximum amplitude of the positive magnetoresistance is about 3.0% at 5 K and 17.5 T. This temperature evolution of magnetoresistance is consistent with the results of temperature dependent
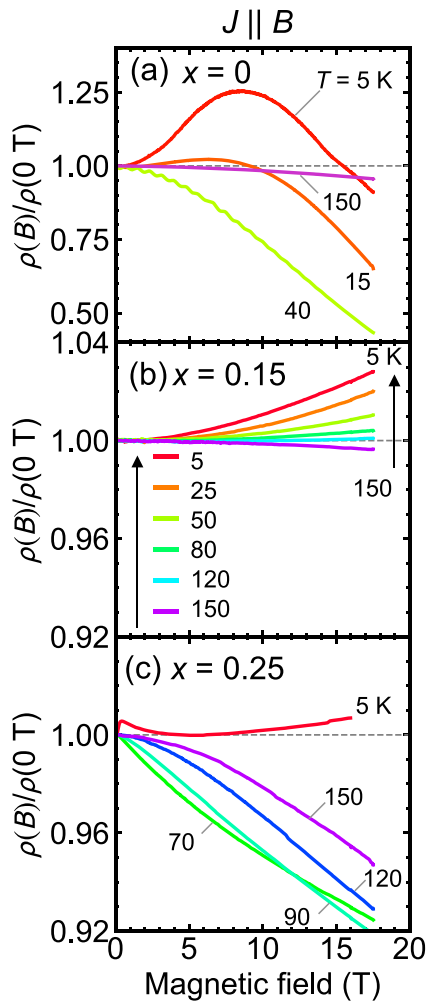
FIG. 4. Isothermal magnetoresistance up to 17.5 T with the configuration of $J||B||100$ for Ba$_{1-x}$K$_x$Mn$_2$As$_2$. (a) $x = 0$, (b) $x = 0.15$, and (c) $x = 0.25$.

FIG. 5. Isothermal magnetoresistance with the configuration of $J||100$ for Ba$_{1-x}$K$_x$Mn$_2$As$_2$ with $x = 0.30$. The magnetic field is (a) $B||100$ and (b) $B||010$.

D. Angle dependence of magnetoresistance

In the isothermal condition, a characteristic anisotropy was observed in magnetoresistance. Thus, we measured ρ in a rotating magnetic field of 17.5 T in the ab plane as shown in the inset of Fig. 6(b). The results of angle dependence at $x = 0$ are shown in Fig. 6(a). At 210 K, ρ at $\theta = 90°$ and $270°$ are smaller than that at $\theta = 0°$ and $180°$. With cooling down to 20 K, its sign reverses; ρ at $\theta = 90°$ and $270°$ are larger than that at $\theta = 0°$ and $180°$ below 20 K. A maximum anisotropy of 3% was observed at 15 K, the lowest temperature measured. This angle dependence is suppressed by the hole doping, and no significant anisotropy was observed for $x = 0.15$ [Fig. 6(b)]. The anisotropy of magnetoresistance was observed again at $x = 0.25$, which is ferromagnetic below 100 K, as shown in Fig. 6(c). At 210 K, ρ at $\theta = 90°$ and $270°$ are smaller than that at $\theta = 0°$ and $180°$. With decreasing temperature, the anisotropy becomes more pronounced, and a slight decrease in ρ was observed around $\theta = 0°$ and $180°$ below the ferromagnetic transition temperature, suggesting the emergence of higher-order anisotropy. To quantify the anisotropy in magnetoresistance, we introduce a fitting model on the basis of the group theory [23],

$$\rho(17.5 \text{ T}, \theta)/\rho(0, 0) = A_{\text{const.}} + A_{2\theta} \cos 2\theta + A_{4\theta} \cos 4\theta. \tag{1}$$

The fitting results using this phenomenological model are shown by a solid line in Figs. 6(a)–6(c), which reproduces well the experimental results. The temperature dependence of the fitting coefficients is shown in Figs. 7(a)–7(c). The $A_{\text{const.}}$ term, which represents an isotropic contribution to magnetoresistance, strongly depends on the x values. The $|A_{\text{const.}}|$ term monotonically increases on cooling at $x = 0$ and 0.15; however, its signs are opposite between two compositions. At $x = 0.25$, the $A_{\text{const.}}$ term has negative value with a minimum at around the ferromagnetic transition temperature $\sim$100 K. The $A_{2\theta}$ term, which represents the lowest-order anisotropy in magnetoresistance, is sizable below the characteristic temperature of $T^\star \sim 20$ K at $x = 0$ and the ferromagnetic transition

experiments shown in Fig. 3(b). In $x = 0.25$ [Fig. 4(c)], a negative magnetoresistance is observed in 120–210 K. With cooling, the negative magnetoresistance develops with a maximum value of 8% at around 90 K, which is close to the ferromagnetic transition temperature. With further cooling, the negative magnetoresistance starts to be suppressed, and the data curvature changes downwardly with respect to the magnetic field below 90 K. Additionally, a positive magnetoresistance is observed in a weak magnetic field region less than 1 T below 90 K.

We next investigate the difference of magnetoresistance between longitudinal and transverse geometries with a particular focus on the weak magnetic field regions. Figure 5 represents the magnetoresistance below $B = \pm 3$ T at $x = 0.30$, which shows ferromagnetic transition at 100 K (data not shown). A sharp structure was observed at around zero field below 100 K. In the longitudinal configuration, the magnetoresistance has a steep dip structure at zero field, while in the transverse configuration, the magnetoresistance has a peak structure at zero field. Hence, it is evident that there is directional anisotropy in the magnetoresistance.
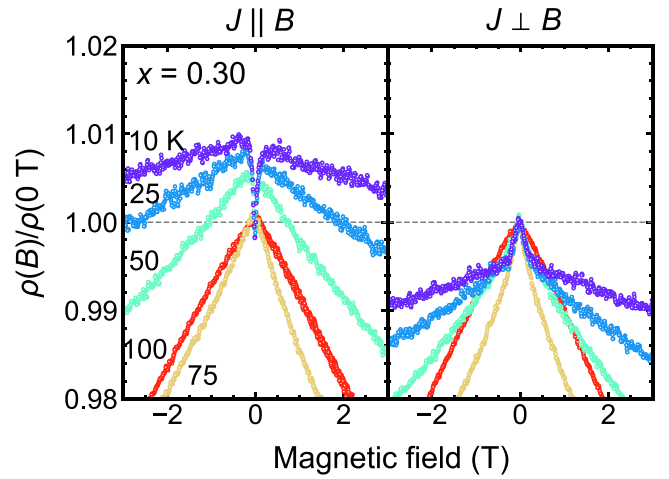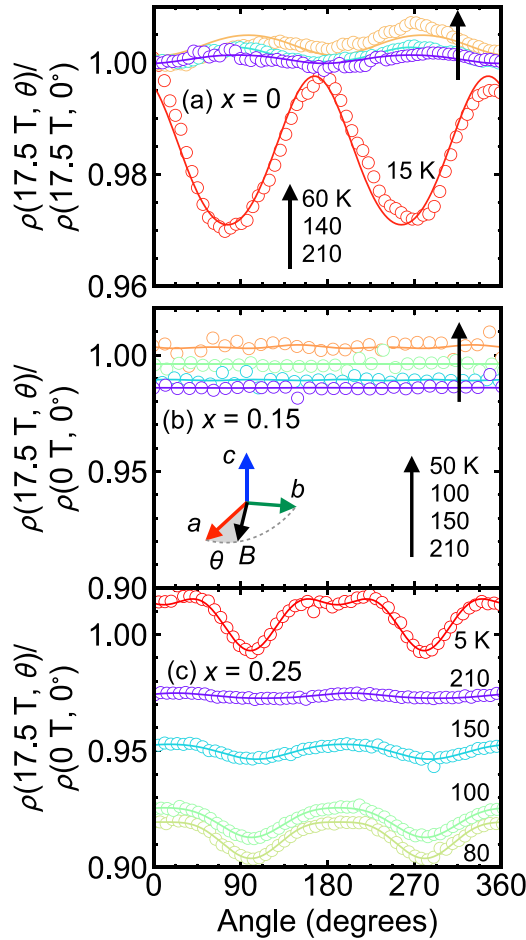
FIG. 6. Angle dependence of magnetoresistance with the configuration of $J||100$ for $Ba_{1-x}K_xMn_2As_2$ with $x = 0$ (a), $x = 0.15$ (b), and $x = 0.25$ (c). The external magnetic field of 17.5 T is rotated in ab plane as described in an inset of (b). The solid lines are the fitting results of the phenomenological model (see the main text for details).

FIG. 7. The temperature dependence of the fitting parameters in analyzing the angle dependence of magnetoresistance for $Ba_{1-x}K_xMn_2As_2$. Here a phenomenological model $\rho(17.5\ T, \theta)/\rho(0, 0) = A_{const.} + A_2 \cos 2\theta + A_4 \cos 4\theta$ is used for fitting the data presented in Fig. 6. The light solid lines are the guide for eyes.

temperature of 100 K at $x = 0.25$, whereas it is negligible in the whole temperature ranges at $x = 0.15$. The $A_{4\theta}$ term, which represents the higher-order anisotropy in magnetoresistance, is only observable at $x = 0.25$. The $A_{4\theta}$ term develops below the ferromagnetic transition temperature of 100 K; this corresponds to the slight reduction of ρ observed around $0°$ and $180°$ in angle dependence of magnetoresistance in $x = 0.25$.

IV. DISCUSSION

A. Origin of magnetoresistance effect

We will discuss the microscopic mechanism of the magnetoresistance. We claim that the observed magnetoresistance can be understood as a sum of three contributions: (1) the positive magnetoresistance induced by an external magnetic field, (2) the negative magnetoresistance induced by the suppressed spin fluctuations, and (3) the positive magnetoresistance induced by a spin-orbit coupling. The ob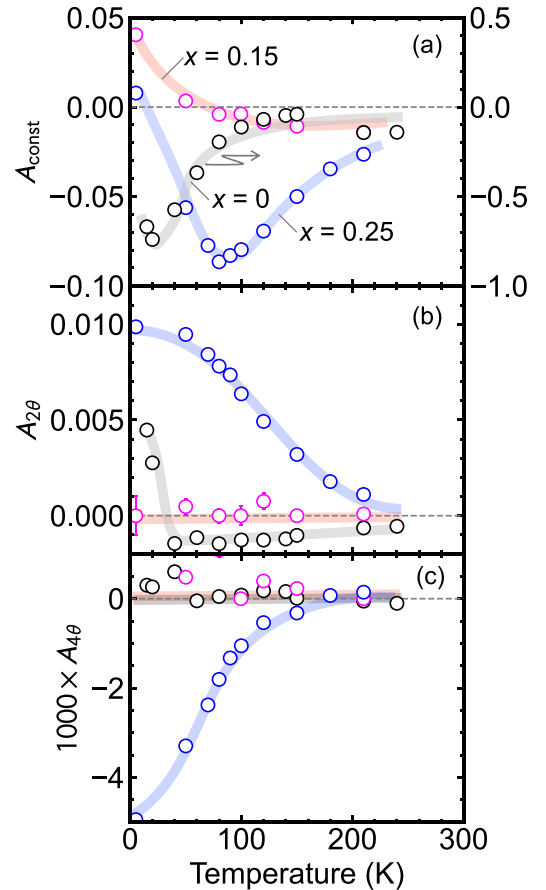served complex magnetoresistance depending on the chemical composition and temperature can be well explained by these multiple contributions as described in the following.

To begin with, let us discuss the effect of the external magnetic field. The most noticeable effect of the external magnetic field is the normal magnetoresistance due to the cyclotron motion of carriers in metals. The positive magnetoresistance at $x = 0.15$, which is the antiferromagnetic metal in whole temperature ranges, is attributable to this effect, because the observed magnetoresistance is proportional to the square of the magnetic field and increases on cooling following the Kohlar's rule [Figs. 3(b) and 4(b)]. The positive magnetoresistance observed below 20 K at $x = 0.25$ most likely has the same origin [Figs. 3(b) and 4(c)]. The positive magnetoresistance observed below the characteristic temperature of $T^\star \sim 20$ K at $x = 0$ might be related to this effect; however, one cannot apply the concept of the cyclotron motion of carriers to $x = 0$ straightforwardly, since the compound exhibits an insulating behavior below $T^\star$. Instead, we should consider the hopping conduction. The external magnetic field bears the Zeeman splitting of the localized carriers. Consequently, the hopping carriers, which are strongly coupled to

the localized spins via the exchange interaction, are influenced by the external magnetic field. In such a case, it is known that the hopping carriers show the positive magnetoresistance [24]. The observed positive magnetoresistance at $x = 0$ can be interpreted in this manner.

Next, we discuss the magnetoresistance caused by spin fluctuations. In ferromagnetic metals, spin fluctuations work as scattering sources for conduction electrons. Around the ferromagnetic transition temperature, therefore, the large negative magnetoresistance is often observed owing to the magnetic field induced suppression of spin fluctuations [25,26]. The colossal magnetoresistance in double exchange systems is a good example. This mechanism well explains the negative magnetoresistance at $x = 0.25$ [Fig. 3(b)], which peaks near the ferromagnetic transition temperature. The negative magnetoresistance observed over a wide temperature range at $x = 0$ is also related to this effect; however, one cannot directly apply the ferromagnetic spin fluctuation scenario to $x = 0$, since the compound does not show any ferromagnetic transitions. Instead, we consider the magnetic field induced suppression of the antiferromagnetic spin fluctuation [27]. In BaMn$_2$As$_2$, a small hole pocket near the Γ point is responsible for the electronic conduction, and therefore magnons with a small wave number dominantly contribute to the electron-magnon scattering. The application of a magnetic field in the ab plane increases the spin gap at the zero wave number in the magnon dispersion, which suppresses the electron-magnon scattering. This results in a negative magnetoresistance. This effect is superimposed on the positive magnetoresistance caused by the external magnetic field, therefore, we observe a peak structure in an isothermal magnetoresistance below $T^\star$ [Fig. 4(a)] at $x = 0$.

Finally, we discuss the magnetoresistance induced by the spin-orbit coupling. In the $(3d)^5$ electron configuration of Mn^{2+} ions, the local orbital angular momentum should be quenched, so that one might imagine that the effect of the spin-orbit interaction is limited. However, since Wannier orbitals in this system are composed of the strongly hybridized Mn d and As p orbitals, reasonable contributions of the spin-orbit coupling to the magnetoresistance are expected The most distinctive magnetotransport induced by the spin-orbit coupling is an anisotropic magnetoresistance (AMR), which is a difference of ρ between longitudinal and transverse configurations in ferromagnetic metals. A simple interpretation of AMR is that the scattering probability of a spin-polarized conduction electron by a nonmagnetic impurity depends on the magnetization direction. In other words, electron orbitals are distorted by the spin-orbit coupling depending on the magnetization direction, which increases/decreases the density of states in the final state of the scattering process. These mechanism results in a peculiar angular dependence of the electrical resistance, and the AMR is typically positive in the longitudinal geometry [25,28,29]. This consideration well explains the observed anisotropic features of the magnetoresistance in the ferromagnetic phase in $x = 0.25$ and 0.30, which are characterized by the temperature evolution of $A_{2\theta}$ and $A_{4\theta}$ below the ferromagnetic transition temperature. In $x = 0$, since the $A_{2\theta}$ term increases toward to the high resistive region [Fig. 7(a)], the observed angle dependence of magnetoresistance can be interpreted as AMR at the dirty limit.

B. Anisotropic magnetoresistance originating from odd-parity multipole order

As discussed in the previous subsection, the angle dependence of magnetoresistance is understood on the basis of the scattering theory for AMR; however, in the present case, it can be understood more straightforwardly by considering magnetic multipoles. Under the magnetic point group $4'/m'mm'$ in the magnetically ordered phase of BaMn$_2$As$_2$, magnetic quadrupole of $xS_x - yS_y$ and the magnetic hexadecapole of $(x^2 - y^2)_z S_z$ arise as the leading and secondary order parameters [30,31]. In such a phase, the magnetoelectric coupling with $P_a = \alpha_{aa}B_a$ and $P_b = -\alpha_{aa}B_b$ (P_i being the polarization, and alpha being the magnetoelectric tensor) is allowed, so that the application of a magnetic field produces a polar axis in the crystal. Owing to the orthorhombic distortion caused by the polar axis in the ab plane, the band dispersions in the a and b directions are inequivalent, resulting in a difference in the effective mass of electrons for each direction, which work as the source of the AMR. Especially, this magentoelectric effect mechanism for AMR works well in $x = 0$ without a ferromagnetic transition. Actually, the observed enhancement of AMR in the insulating regime at low temperatures strongly supports the contribution of this mechanism. However, at present, this tentative scenario is not verified because of the lack of information regarding the orthorhombic modification of the Fermi surface. To confirm this scenario, a relativistic band calculation and a direct observation of Fermi surface via the angle-resolved photoemission or Shubnikov–De Haas effect experiments are needed.

V. SUMMARY

In summary, we examined the magnetoresistance (MR) in Ba$_{1-x}$K$_x$Mn$_2$As$_2$, which exhibit simultaneous breaking of the spatial-inversion and the time-reversal symmetries owing to the magnetic ordering. Our experiments cover three characteristic electronic phases: an antiferromagnetic insulating phase, an antiferromagnetic metallic phase, and a parasitic-ferromagnetic metallic phase. In the antiferromagnetic insulating phase, we observed a nonmonotonic field dependence of magnetoresistance with a sizable anisotropy. In the antiferromagnetic metallic phase, we observed the monotonic field dependence of magnetoresistance proportional to the square of the magnetic field, which shows negligible angular dependencies. In the parasitic-ferromagnetic metallic phase, we observed a sharp dip/peak structures in the magnetoresistance at zero filed; moreover, we observed a high-order anisotropic magnetoresistance. These experimental results are discussed in terms of three contributions based on scattering theory: the magnetoresistance due to (1) the external magnetic field, (2) the spin fluctuations, and (3) the spin-orbit interaction. Finally, we propose the possibility of anisotropic magnetoresistance due to the Fermi surface warping via the magnetoelectric effect derived from odd-parity magnetic multipoles.

[1] P. Wadley, B. Howells, J. Železný, C. Andrews, V. Hills, R. P. Campion, V. Novák, K. Olejník, F. Maccherozzi, S. S. Dhesi, S. Y. Martin, T. Wagner, J. Wunderlich, F. Freimuth, Y. Mokrousov, J. Kuneš, J. S. Chauhan, M. J. Grzybowski, A. W. Rushforth, K. Edmond *et al.*, Science **351**, 587 (2016).

[2] H. Saito, K. Uenishi, N. Miura, C. Tabata, H. Hidaka, T. Yanagisawa, and H. Amitsuka, J. Phys. Soc. Jpn. **87**, 033702 (2018).

[3] Y. Shiomi, H. Watanabe, H. Masuda, H. Takahashi, Y. Yanase, and S. Ishiwata, Phys. Rev. Lett. **122**, 127207 (2019).

[4] S. Hayami, M. Yatsushiro, Y. Yanagi, and H. Kusunose, Phys. Rev. B **98**, 165110 (2018).

[5] Y. Singh, A. Ellern, and D. C. Johnston, Phys. Rev. B **79**, 094519 (2009).

[6] J. An, A. S. Sefat, D. J. Singh, and M. H. Du, Phys. Rev. B **79**, 075120 (2009).

[7] Y. Singh, M. A. Green, Q. Huang, A. Kreyssig, R. J. McQueeney, D. C. Johnston, and A. I. Goldman, Phys. Rev. B **80**, 100403(R) (2009).

[8] D. C. Johnston, R. J. McQueeney, B. Lake, A. Honecker, M. E. Zhitomirsky, R. Nath, Y. Furukawa, V. P. Antropov, and Y. Singh, Phys. Rev. B **84**, 094445 (2011).

[9] H. Watanabe and Y. Yanase, Phys. Rev. B **96**, 064432 (2017).

[10] K. Ohgushi *et al.*, J. Phys. Soc. Jpn. (unpublished).

[11] J. K. Bao, H. Jiang, Y. L. Sun, W. H. Jiao, C. Y. Shen, H. J. Guo, Y. Chen, C. M. Feng, H. Q. Yuan, Z. A. Xu, G. H. Cao, R. Sasaki, T. Tanaka, K. Matsubayashi, and Y. Uwatoko, Phys. Rev. B **85**, 144523 (2012).

[12] A. Pandey, R. S. Dhaka, J. Lamsal, Y. Lee, V. K. Anand, A. Kreyssig, T. W. Heitmann, R. J. McQueeney, A. I. Goldman, B. N. Harmon, A. Kaminski, and D. C. Johnston, Phys. Rev. Lett. **108**, 087005 (2012).

[13] J. Lamsal, G. S. Tucker, T. W. Heitmann, A. Kreyssig, A. Jesche, A. Pandey, W. Tian, R. J. McQueeney, D. C. Johnston, and A. I. Goldman, Phys. Rev. B **87**, 144418 (2013).

[14] S. Yeninas, A. Pandey, V. Ogloblichev, K. Mikhalev, D. C. Johnston, and Y. Furukawa, Phys. Rev. B **88**, 241111(R) (2013).

[15] A. Pandey, B. G. Ueland, S. Yeninas, A. Kreyssig, A. Sapkota, Y. Zhao, J. S. Helton, J. W. Lynn, R. J. McQueeney, Y. Furukawa, A. I. Goldman, and D. C. Johnston, Phys. Rev. Lett. **111**, 047001 (2013).

[16] B. G. Ueland, A. Pandey, Y. Lee, A. Sapkota, Y. Choi, D. Haskel, R. A. Rosenberg, J. C. Lang, B. N. Harmon, D. C. Johnston, A. Kreyssig, and A. I. Goldman, Phys. Rev. Lett. **114**, 217001 (2015).

[17] J. K. Glasbrenner and I. I. Mazin, Phys. Rev. B **89**, 060403(R) (2014).

[18] K.-K. Huynh, T. Ogasawara, K. Kitahara, Y. Tanabe, S. Y. Matsushita, T. Tahara, T. Kida, M. Hagiwara, D. Arčon, and K. Tanigaki, Phys. Rev. B **99**, 195111 (2019).

[19] T. Ogasawara, K.-K. Huynh, T. Tahara, T. Kida, M. Hagiwara, D. Arčon, M. Kimata, S. Y. Matsushita, K. Nagata, and K. Tanigaki, Phys. Rev. B **103**, 125108 (2021).

[20] T. Holstein, Ann. Phys. **8**, 343 (1959).

[21] I. Austin and N. Mott, Adv. Phys. **18**, 41 (1969).

[22] N. Janša, K.-K. Huynh, T. Ogasawara, M. Klanjšek, P. Jeglič, P. Carretta, K. Tanigaki, and D. Arčon, Phys. Rev. B **103**, 064422 (2021).

[23] R. R. Birss, *Symmetry and Magnetism*, 2nd ed. (North-Holland, Amsterdam, 1966).

[24] H. Kamimura, A. Kurobe, and T. Takemori, Physica B **118**, 652 (1983).

[25] T. McGuire and R. Potter, IEEE Trans. Magn. **11**, 1018 (1975).

[26] P. F. Bongers, C. Haas, A. M. Van Run, and G. Zanmarchi, J. Appl. Phys. **40**, 958 (1969).

[27] H. Li, Phys. Rev. B **85**, 134426 (2012).

[28] J. Kondo, Prog. Theor. Phys **27**, 772 (1962).

[29] S. Kokado, M. Tsunoda, K. Harigaya, and A. Sakuma, J. Phys. Soc. Jpn. **81**, 024705 (2012).

[30] A. Shitade, H. Watanabe, and Y. Yanase, Phys. Rev. B **98**, 020407(R) (2018).

[31] H. Watanabe and Y. Yanase, Phys. Rev. Research **2**, 043081 (2020).